Nonbiological Fractionation of Iron Isotopes

A. D. Anbar,[1,2]* J. E. Roe,[2] J. Barling,[1] K. H. Nealson[3]

Laboratory experiments demonstrate that iron isotopes can be chemically fractionated in the absence of biology. Isotopic variations comparable to those seen during microbially mediated reduction of ferrihydrite are observed. Fractionation may occur in aqueous solution during equilibration between inorganic iron complexes. These findings provide insight into the mechanisms of iron isotope fractionation and suggest that nonbiological processes may contribute to iron isotope variations observed in sediments.

Because of the small relative mass difference among Fe isotopes (masses 54, 56, 57, and 58), fractionations by simple chemical processes are expected to be small. The isotopic composition of Fe extracted from a variety of igneous rocks shows no measurable variation, consistent with this expectation (*1*). In contrast, laboratory studies indicate that the isotopic composition of Fe(II) produced by dissimilatory Fe-reducing bacteria grown on ferrihydrite is about 0.5‰ per atomic mass unit lighter than Fe(III) in the growth media (*2*, *3*). Hence, it has been hypothesized that only metabolic processes, which involve multiple steps, produce substantial Fe isotope fractionation, and that isotopic variations observed in recent and ancient sediments indicate biological processing of Fe (*2*). However, equilibrium isotope fractionation factors decrease with increasing temperature (*4*), and the environmental chemistry of Fe also involves multiple steps. Therefore, the results from igneous rocks do not exclude the possibility that the variations in sediments are of nonbiological origin.

Here, we show that Fe isotope fractionation can occur as the result of chemical processes at room temperature in the absence of biology. Isotopic compositions were measured by multiple collector–inductively coupled plasma–mass spectrometry (MC-ICP-MS) (*5*–*9*) with a desolvation system (*10*). This approach permits precise determination of δ^{56}Fe and δ^{57}Fe (*11*). In our experimental systems, we used a strongly basic anion exchange resin consisting of a styrene divinylbenzene backbone with positively charged functional groups [R-$CH_2N^+(CH_3)_3$]. In acidic aqueous solutions with high Cl^- activities, Fe forms a series of chloro-complexes, including $FeCl_4^-$ which binds strongly but reversibly to these functional groups (*12*, *13*). Partitioning of Fe(III) between dissolved and bound forms is governed by a conditional distribution coefficient, $K_D = C_r/C_s$, where C_r is the concentration of resin-bound Fe ($FeCl_4$ − R) and C_s is the concentration of Fe in solution (*14*). Mass-dependent differences in K_D can lead to isotope fractionation between dissolved and bound Fe. Therefore, any fractionation observed in our experiments is strictly nonbiological and can be related to equilibration between dissolved Fe(III) complexes and resin-bound Fe.

Chromatographic experiments were conducted to explore the mass-dependent variability of K_D (*15*). Chromatographic isotope fractionation is well known for some ions (*5*, *16*–*18*). Here, Fe(III) was loaded on an ion-exchange column in 7 M HCl. Because $FeCl_4^-$ is a major species under these conditions, the $K_D \sim 1400$ (*19*) and the loaded Fe was confined to the top of the column. The Fe was eluted by reducing the HCl concentration, which lowers the K_D by shifting the equilibrium solution speciation to $FeCl_3$ and $FeCl_2^+$ (*13*, *19*). The eluate was collected in a series of fractions that totaled ~100% of the loaded Fe. The rate at which ^{54}Fe and ^{56}Fe elute from the column depends, to first order, on the relative magnitudes of $^{54}K_D$ and $^{56}K_D$. Relative to the isotopic composition of the Fe loaded on the column, early elution fractions will be enriched in the isotope with the smaller K_D, whereas the last fractions will be enriched in the isotope with the larger K_D.

We observed variations in the isotopic composition of Fe in a series of chromatographic experiments. The earliest Fe eluted from the column was always enriched in the heavier isotope ($\delta^{56}Fe > 0$), whereas the later fractions were depleted ($\delta^{56}Fe < 0$) compared with the Fe loaded on the column ($\delta^{56}Fe = 0$). Hence, $^{54}K_D/^{56}K_D > 1$. In a typical experiment (Fig. 1), δ^{56}Fe ranged from 3.6 to −3.4‰. This is a larger range of variation than observed in natural samples or in microbial Fe-reduction experiments (*2*, *3*, *20*).

Because both δ^{56}Fe and δ^{57}Fe were determined, we can verify that the observed δ^{56}Fe variations result from mass-dependent fractionation rather than from isobaric interferences. We find $\delta^{56}Fe \sim 0.68 \times \delta^{57}Fe$ ($r^2 = 0.99$), which is consistent with theory (*21*). Additional verification is provided by mass balance, which requires that the isotopic composition of the eluted Fe integrated over all elution fractions should be identical to that of the loaded Fe if 100% of the loaded Fe is recovered. This expectation is confirmed in our system, where δ^{56}Fe and δ^{57}Fe are ~0 when the cumulative yield is ~100%.

Chromatographic data can be related to $^{54}K_D/^{56}K_D$ and $^{54}K_D/^{57}K_D$ by recognizing that the δ^{56}Fe and δ^{57}Fe data reflect the superposition of three independent elution curves, corresponding to the elution of ^{54}Fe, ^{56}Fe, and ^{57}Fe. The separation between these curves can be estimated and related to the distribution coefficients by plotting the isotopic composition of each elution fraction against cumulative eluted percent on a probability abscissa (*17*, *18*) (Fig. 2). Using this approach, the data are consistent with $^{54}K_D/^{56}K_D \sim 1.0001$ and $^{54}K_D/^{56}K_D \sim 1.00015$ (*22*).

Differences in metal coordination between equilibrated species could give rise to such effects (*23*). This provides a framework for interpretation of Fe isotope fractionation in our experiments. For example, during elution in 2 M HCl, >90% of dissolved Fe is present as $FeCl_2^+$, $FeCl_3$, and $FeCl_4^-$ (*13*). Hence, the most important equilibria governing the distribution between dissolved and resin-bound Fe in our systems are likely $FeCl_2^+ + Cl^- \leftrightarrow FeCl_3$ (K_1); $FeCl_3 + Cl^- \leftrightarrow FeCl_4^-$ (K_2); and $FeCl_4^- + R - Cl \leftrightarrow FeCl_4^- - R + Cl^-$ (K_R). From the equilibrium expressions for these reactions, given $K_1 \sim 0.15$, $K_2 \sim 0.01$, and $a_{Cl} \sim 2$ M (*13*), it can be shown that $^{54}K_D/^{56}K_D \sim {}^{54}K_1/^{56}K_1 \times {}^{54}K_2/^{56}K_2 \times {}^{54}K_R/^{56}K_R$. There is little difference in metal coordination between $FeCl_4^-$ and $FeCl_4$ − R. In addition, the relative mass difference between $^{54}FeCl_4^-$ and $^{56}FeCl_4^-$ (~ 1%) is small. Therefore, it is likely that fractionation does not occur during binding to the resin and that $^{54}K_D/^{56}K_D \sim {}^{54}K_1/^{56}K_1 \times {}^{54}K_2/^{56}K_2$. There is a large difference in coordination between $FeCl_2^+$ and $FeCl_4^-$ (*24*, *25*); the latter is tetrahedrally coordinated, whereas the former is octahedral [$FeCl_2(H_2O)_4^+$]. The coordination of $FeCl_3$ is less certain (*13*, *24*, *25*), but may also be octahedral [$FeCl_3(H_2O)_3$]. If so, we suspect that $^{54}K_2/^{56}K_2 > {}^{54}K_1/^{56}K_1 = 1$. If $^{54}K_D/^{56}K_D \sim 1.0001$, then α, the equilibrium fractionation factor, ~1.0001 for the isotope exchange reaction $^{54}FeCl_3 + {}^{56}FeCl_4^- \leftrightarrow {}^{56}FeCl_3 + {}^{54}FeCl_4^-$. Alternatively, it is possible that $^{54}K_1/^{56}K_1 > {}^{54}K_2/^{56}K_2 = 1$ or that $^{54}K_1/^{56}K_1 \sim {}^{54}K_2/^{56}K_2 \neq 1$. In the former case, $\alpha \sim 1.0001$ for $^{54}FeCl_2^+ + {}^{56}FeCl_3 \leftrightarrow {}^{56}FeCl_2^+ + {}^{54}FeCl_3$. In the latter case, $\alpha \sim 1.00005$ for each reaction.

[1]Department of Earth and Environmental Sciences, [2]Department of Chemistry, University of Rochester, Rochester, NY 14627, USA. [3]Jet Propulsion Laboratory, California Institute of Technology, Pasadena, CA 91106, USA.

*To whom correspondence should be addressed. E-mail: anbar@earth.rochester.edu

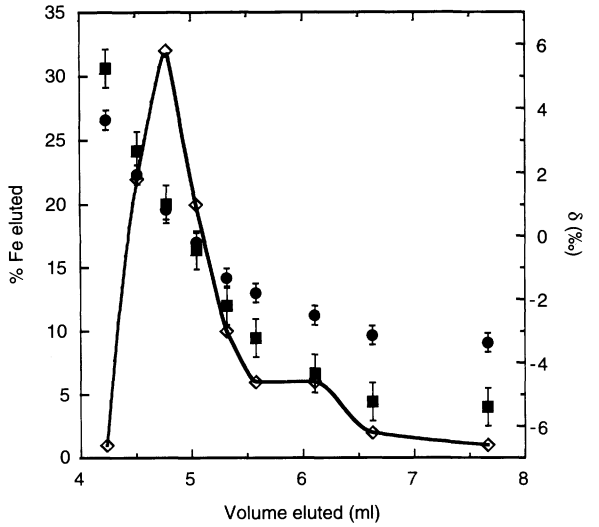

Fig. 1 (left). $\delta^{56}Fe$ (●) and $\delta^{57}Fe$ (■) versus volume eluted in a typical chromatographic experiment (*15*). For Fe loaded on the column, $\delta^{56}Fe = \delta^{57}Fe \equiv 0‰$. (◇) percent of total Fe recovered in each fraction; the cumulative yield was 100%. Integrated over all elution fractions, cumulative $\delta^{56}Fe = 0.2 \pm 0.3‰$ and cumulative $\delta^{57}Fe = 0.0 \pm 0.6‰$. Error bars indicate $\pm 2\sigma$ uncertainties.

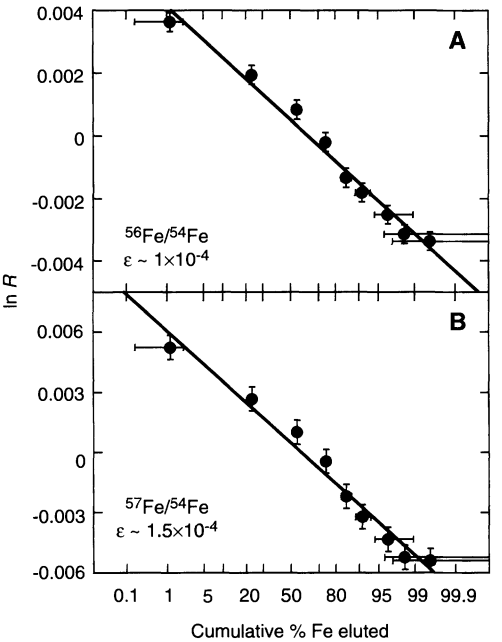

Fig. 2 (right). Isotopic compositions in chromatographic elution fractions (R) plotted against cumulative percent Fe recovered on a probability abscissa (*17*, *18*). $R = (^{M}Fe/^{54}Fe)_{fraction}/(^{M}Fe/^{54}Fe)_{total}$, where $M = 56$ (**A**) or 57 (**B**). The slope on such plots reflects the extent of isotope separation during elution, and is approximately equal to $-\varepsilon\sqrt{N}$. N, the number of theoretical plates in the column (*28*); ε, the single-step ("batch") enrichment factor (*17*, *18*). If isotope separation is the result of equilibration with the resin, $^{54}K_D/^{M}K_D = 1 + \varepsilon$. Error bars indicate $\pm 2\sigma$ uncertainties.

Such a model may explain why $^{54}K_D/^{56}K_D > 1$. Octahedral Fe chloro-aquo complexes may provide stronger bonding environments for Fe than $FeCl_4^-$. Because heavier isotopes partition preferentially into the stronger bonding environment (*23*), the heavier Fe isotopes should preferentially partition into the dissolved phase in our experiments. Additionally, this model is consistent with the absence of isotope fractionation in Fe and Zn anion chromatography experiments in which these elements were eluted with the use of very dilute acids (*1*, *5*). In the case of Fe, $FeCl_4^-$ only becomes an important species when the concentration of HCl > 1 M. Therefore, elution with dilute acid should lead to nearly quantitative conversion of Fe to neutral and cationic complexes, and hence little mass-dependent separation during elution. Similar logic applies to Zn. In contrast, fractionation has been observed during elution of Cu in 7 M HCl (*5*).

Isotope fractionations are expected during equilibration between any two metal complexes with different bonding energetics (*4*, *23*), as may occur during reactions that change coordination geometry (as suspected here), ligand identities, or metal redox state. Such reactions are common in the biogeochemistry of Fe. For example, redox reactions that convert Fe(II) to Fe(III) (and vice versa) are common in the environment and in biology. Dissolution and precipitation of minerals such as magnetite and chalcopyrite involves conversion between dissolved octahedrally coordinated Fe and Fe(III) in tetrahedral coordination in the minerals. In the uptake of Fe by many microorganisms, inorganically or organically complexed Fe(III) is converted to extremely stable organic complexes that are taken up by specific transport mechanisms (*26*). Within cells, reduction of Fe(III) to Fe(II) is often necessary to release Fe from the organic ligand, and octahedral Fe complexes must be converted to tetrahedral coordination in Fe-S proteins. All these reactions involve changes in Fe bonding energetics comparable to, or larger than, those between the Fe chloro-complexes studied here. Hence, equilibrium fractionation factors ≥1.0001 may be common in Fe chemistry, with larger effects likely for unidirectional reactions. Thus, our results suggest that fractionations of ~1‰ observed in biological systems could result from a small number of key changes in speciation during Fe uptake and metabolism. At the same time, separation of different Fe species during ion exchange, ion adsorption, or the precipitation of insoluble phases may lead to similar Fe isotope variations in the environment even in the absence of biology, especially if Rayleigh fractionation is involved (*27*). Hence, nonbiological processes may contribute to the variations in Fe isotopic composition observed in modern and ancient sediments.

References and Notes

1. B. L. Beard and C. M. Johnson, *Geochim. Cosmochim. Acta* **63**, 1653 (1999).
2. B. L. Beard *et al.*, *Science* **285**, 1889 (1999).
3. T. D. Bullen and P. M. McMahon, *Mineral. Mag.* **62A**, 255 (1998).
4. H. C. Urey, *J. Chem. Soc.* **1947**, 562 (1947); V. B. Polyakov and S. D. Mineev, *Geochim. Cosmochim. Acta.* **64**, 849 (2000).
5. C. N. Marechal *et al.*, *Chem. Geol.* **156**, 251 (1999).
6. A. N. Halliday *et al.*, *Int. J. Mass Spectrom. Ion Processes* **146**, 21 (1995).
7. A. D. Anbar *et al.*, *Mineral. Mag.* **62A**, 53 (1998).
8. X. K. Zhu *et al.*, *Chem. Geol.* **163**, 139 (2000).
9. Mass spectrometric analyses were conducted with a MC-ICP-MS (Plasma 54; VG Elemental, Winsford, UK). The Fe isotopic composition of each sample is compared with that of a standard solution (Specpure, Johnson Matthey, London) and is reported as $\delta^{56}Fe$ and $\delta^{57}Fe$ $\{\delta^{M}Fe = [(^{M}Fe/^{54}Fe)_{sample}/(^{M}Fe/^{54}Fe)_{standard} - 1] \times 1000‰$, where $M = 56$ or 57$\}$. We used an "elemental spike" approach to correct for instrumental mass bias; Cu (masses 63 and 65) was added to both samples and standards, and analyses of standards were interleaved with samples. Fe and Cu isotopes were analyzed in alternate cycles.
10. Samples were introduced with a desolvation system (Aridus I; CETAC Technologies, Omaha, NE). Desolvation was necessary to keep isobaric interferences from ArO^+ and ArN^+ to <1‰ (<5 mV) and <6‰ (<2 mV) of the signals at Fe masses 56 and 54, respectively. The contribution from $ArOH^+$ (mass 57) was negligible. The residual ArO^+ and ArN^+ ion beams were typically stable to better than ±5% over several hours, so correction was possible with less than ~0.3‰ uncertainty. The contribution of this uncertainty to $\delta^{56}Fe$ and $\delta^{57}Fe$ was minimized by matching the intensities of sample and standard ion beams with appropriate dilutions. Hence, even a large systematic error in the correction would contribute very similar proportional errors to $(^{M}Fe/^{54}Fe)_{sample}$ and $(^{M}Fe/^{54}Fe)_{standard}$, producing negligible systematic error in $\delta^{M}Fe$.
11. Repeat analyses of a gravimetrically prepared ^{54}Fe-enriched standard over a 6-month period yielded $\delta^{56}Fe = -11.8 \pm 0.2‰$ and $\delta^{57}Fe = -11.8 \pm 0.4‰$ ($\pm 2\sigma$ external precision), versus known values of $-11.8 \pm 0.2‰$ for both ratios. The precision of $\delta^{57}Fe$ determination was somewhat worse than that of $\delta^{56}Fe$ because of the low abundance of ^{57}Fe. In general, the reproducibility of small numbers of repeat analyses of standards and of samples processed through chemistry was similar to these values. We assigned $\pm 2\sigma$ uncertainties of ±0.3‰ ($\delta^{56}Fe$) and ±0.6‰ ($\delta^{57}Fe$) to single analyses of chemically processed samples.
12. G. E. Moore and K. A. Kraus, *J. Am. Chem. Soc.* **72**, 5792 (1959).
13. J. Bjerrum and I. Lukes, *Acta Chem. Scand. Ser. A* **40**, 31 (1986).
14. D. A. Skoog *et al.*, in *Instrumental Analysis* (Saunders College Publishing, Chicago, 1998), pp. 675–697.
15. In a typical chromatographic experiment, Fe(III) (~200 μg; Specpure) was dissolved in 1 ml of 7 M HCl + 0.001% H_2O_2. The solution was loaded onto ~2 ml of resin (AG MP-1; Bio-Rad, Hercules, CA)

packed in a polypropylene column (0.5 cm^2 × 3.7 cm). Fe was entirely eluted with ~8 ml of 2 M HCl + 0.001% H_2O_2, flowing at a rate of ~0.3 ml/min. The eluate was collected in a series of fractions, ranging in size from 0.2 to 2 ml. Elution fractions were dried and redissolved in 1 ml of 0.05 M HNO_3. About 20% of each solution was used to determine Fe concentrations by ultraviolet–visible light spectrophotometry. The remainder was diluted to a concentration of ~3 parts per million Fe for isotopic analysis. All experiments were conducted in a clean lab with acid-cleaned Teflon labware, acid-cleaned resin, and ultrapure reagents.

16. T. I. Taylor and H. C. Urey, *J. Chem. Phys.* **6**, 429 (1938).
17. W. A. Russell and D. A. Papanastassiou, *Anal. Chem.* **50**, 1151 (1978).
18. E. Glueckauf, *Trans. Faraday Soc.* **54**, 1203 (1956).
19. T. N. van der Walt *et al.*, *Solvent Extr. Ion Exch.* **3**, 723 (1985).
20. K. W. Mandernack, D. A. Bazylinski, W. C. Shanks III, T. D. Bullen, *Science* **285**, 1892 (1999).
21. R. E. Criss, *Principles of Stable Isotope Distribution* (Oxford Univ. Press, New York, 1999).
22. These values should be regarded as order-of-magnitude estimates because this treatment is strictly valid only when the number of theoretical plates $>10^3$ (*18*). However, it has been shown to be a reasonable approximation for smaller columns (*17*). In addition, although kinetic effects may either attenuate or amplify isotopic separation, equilibration with ion-exchange resins is generally rapid on the time scales in our experiments, and the kinetics of equilibration between Fe(III) and AG MP-1 resin are at least as rapid as with other anion exchangers (*19*). The kinetics of Fe(III) ligand exchange are also rapid.
23. J. Bigeleisen and M. G. Mayer, *J. Chem. Phys.* **15**, 261 (1947).
24. M. Magini and T. Radnai, *J. Chem. Phys.* **71**, 4255 (1979).
25. M. J. Apted *et al.*, *Geochim. Cosmochim. Acta* **49**, 2081 (1985).
26. J. B. Neilands, *J. Biol. Chem.* **270**, 26723 (1995).
27. T. D. Bullen *et al.*, *Eos* **80**, 479 (1999).
28. From an ideal Gaussian elution curve, N, the number of theoretical plates in the column, is readily obtained from the relation $N = 5.57 \times (v_R/W_{1/2})^2$, where v_R is the volume to the curve peak and $W_{1/2}$ is the width of the curve at half-height (*14*). Here, if we neglect tailing, N ~250.
29. We thank F. Albarède, M. Anbar, B. Beard, R. Eisenberg, D. Farnsworth, J. Hayes, C. Johnson, J. Morgan, G. Ravizza, G. Rossman, E. Schauble, and G. Wasserburg for discussions. This research was conducted at the ICP-MS Laboratory of the University of Rochester, with support from NSF (EAR 9601929 and CHE 9714282) and the NASA Astrobiology Institute.

18 November 1999; accepted 24 February 2000

Carbon Isotopic Evidence for Methane Hydrate Instability During Quaternary Interstadials

James P. Kennett,[1]* Kevin G. Cannariato,[1] Ingrid L. Hendy,[1] Richard J. Behl[2]

Large (about 5 per mil) millennial-scale benthic foraminiferal carbon isotopic oscillations in the Santa Barbara Basin during the last 60,000 years reflect widespread shoaling of sedimentary methane gradients and increased outgassing from gas hydrate dissociation during interstadials. Furthermore, several large, brief, negative excursions (up to −6 per mil) coinciding with smaller shifts (up to −3 per mil) in depth-stratified planktonic foraminiferal species indicate massive releases of methane from basin sediments. Gas hydrate stability was modulated by intermediate-water temperature changes induced by switches in thermohaline circulation. These oscillations were likely widespread along the California margin and elsewhere, affecting gas hydrate instability and contributing to millennial-scale atmospheric methane oscillations.

Polar ice cores document large oscillations in atmospheric methane (CH_4) associated with Quaternary climate cycles on orbital, millennial, and decadal time scales (*1, 2*). Dramatic warmings during the first few decades of interglacials and interstadials coincided with rapid atmospheric CH_4 increases (*3*). These rises in CH_4 have been attributed to, in one hypothesis, enhanced methanogenesis in tropical wetlands receiving greater precipitation (*1–3*). However, extensive wetlands (*4*) are unlikely to have developed fast enough during sea-level low stands to account for the rapid rate of increase of atmospheric CH_4.

Another potential source of atmospheric CH_4 is methane (gas) hydrate, a solid formed in sediments from water and CH_4 under conditions of high pressure, low temperature, and sufficient gas concentrations (*5*). Large amounts of CH_4 (1×10^{19} to 2×10^{19} g) are stored on continental margins as gas hydrate and free gas trapped beneath (*6*). The majority of this CH_4 has very negative carbon isotopic values [~−65 per mil (‰)] typical for biogenic CH_4 produced by methanogenesis within anoxic sediments (*7*). The depth zone over which hydrates remain stable is dependent on water depth (pressure) and temperature (*8*). Gas hydrate dissociation can result from pressure decrease due to sea-level fall (*9*) or water temperature increase, the latter of which has been suggested for the late Paleocene (*10*) and observed on a small scale in the Gulf of Mexico (*11*). Released CH_4 is transferred to the exchangeable carbon reservoir by diffusion into the water column or by ebullition into the atmosphere as a result of sediment slope failure, sliding, or collapse (*10*).

Little is known about the stability of continental margin gas hydrates during the Quaternary. Decomposition of gas hydrates destabilizes the sediment column by creating abnormally high porosity at depth (*5*). Widespread sediment disruption (slumps, slides, pockmarks) on upper continental margins represents evidence for major CH_4 release from the ocean floor during the late Quaternary (*5, 12, 13*). The extent of this evidence reflects the magnitude of past release of ocean floor CH_4 and its potential to influence climate change. Several workers have attributed gas hydrate dissociation on the continental margins to sea-level fall during the Quaternary (*9*). However, temperature change has not been implicated previously as a potential factor in Quaternary gas hydrate stability, because there has been little previous evidence for Quaternary temperature increases of sufficient magnitude in upper intermediate-waters (400 to 1000 m) (*14*). Indeed, a seafloor source for CH_4 in ice cores has been dismissed, because inferred increases in atmospheric concentrations occurred during warm intervals when sea level, and hence hydrostatic pressure, was higher (*2*). Nevertheless, strong evidence exists for the role of temperature change, related to deep-sea thermohaline circulation switching, in gas hydrate dissociation during the late Paleocene thermal maximum (*10*).

Recent paleoclimatic records from the California margin exhibit the complete sequence of millennial-scale climate oscillations, termed Dansgaard-Oeschger (D-O) cycles, during the last 60 thousand years (kyr) (*15–17*). These are reflected as sea-surface temperature (SST) changes (*16, 17*), linked via the atmosphere with Greenland climate change (*18*), bottom-water oxygenation as indicated by lamination strength (*15*) and benthic foraminiferal assemblages (*15, 19*), and bottom-water temperatures (*16, 20*). Oxygenation switches on the continental margin resulted from changes in intermediate-water ventilation and surface-water productivity related to thermohaline circulation switches (*15, 16, 19–21*).

Here, we present high-resolution planktonic and benthic foraminiferal carbon and

[1]Geological Sciences and Marine Science Institute, University of California, Santa Barbara, CA 93106, USA. [2]Department of Geological Sciences, California State University, Long Beach, CA 90840, USA.

*To whom correspondence should be addressed. E-mail: kennett@geology.ucsb.edu